New Zealand Journal of Marine and Freshwater Research

ISSN: 0028-8330 (Print) 1175-8805 (Online) Journal homepage: http://www.tandfonline.com/loi/tnzm20

Locally generated tsunami along the Kaikoura coastal margin: Part 1. Fault ruptures

Roy A. Walters , Philip Barnes & James R. Goff

To cite this article: Roy A. Walters , Philip Barnes & James R. Goff (2006) Locally generated tsunami along the Kaikoura coastal margin: Part 1. Fault ruptures, New Zealand Journal of Marine and Freshwater Research, 40:1, 1-16, DOI: 10.1080/00288330.2006.9517399

To link to this article: http://dx.doi.org/10.1080/00288330.2006.9517399

Published online: 30 Mar 2010.

New Zealand Journal of Marine and Freshwater Research, 2006, Vol. 40: 1–16
0028–8330/06/4001–0001

Locally generated tsunami along the Kaikoura coastal margin: Part 1. Fault ruptures

ROY A. WALTERS[1]
PHILIP BARNES[2]
JAMES R. GOFF[1]
[1]National Institute of Water and Atmospheric Research Limited
P.O. Box 8602
Christchurch, New Zealand
email: r.walters@niwa.co.nz

[2]National Institute of Water and Atmospheric Research Limited
Private Bag 14901
Wellington, New Zealand

Abstract Tsunami are generated by sudden movements of the ocean bed or by objects such as subaerial landslides and bolides falling into the ocean. An examination of the geophysical setting for the northeast coast of the South Island, New Zealand, identified a substantial potential for submarine fault ruptures and submarine landslides. To examine possible effects of a tsunami, a numerical model was applied to calculate runup and inundation arising from locally-generated tsunami along this section of the coast. The specific events considered were fault ruptures on the Kekerengu Bank Fault and two lesser faults, and a submarine landslide in Kaikoura Canyon. The model is based on the Reynolds-averaged Navier-Stokes (RANS) equation and used a finite element spatial approximation, implicit time integration, a semi-Lagrangian advection approximation, and a simple method for treating non-hydrostatic pressure variations. The results indicate that the different generation events have significant effects on different parts of the coastal margin. For the fault-rupture events, the northern coast of the study area is very exposed to damage from a potential rupture of the Kekerengu Bank Fault. A concern is that the highest waves near Kaikoura would be a result of late arrival of coastally-trapped waves and would be delayed by up to 1.5h after the fault-rupture event.

Keywords tsunami; fault rupture; Kaikoura, New Zealand

M05022; Online publication date 31 January 2006
Received 28 April 2005; accepted 7 September 2005

INTRODUCTION

Tsunami have occurred relatively frequently along the coast of New Zealand in historical times (de Lange & Fraser 1999). They are transient oscillations of sea level with periods much longer than wind waves but shorter than tides, and can be generally classified as long waves. Tsunami can cause coastal flooding, erosion, and loss of life in extreme events, and therefore can be significant coastal hazards. Tsunami hazard assessment requires investigation of runup and inundation owing to both remote tsunami generated along the west coast of South America, and local tsunami generated along the New Zealand coastal margin. Historically, the two largest remote tsunami to arrive in New Zealand were the 1868 and the 1960 Chile tsunami with a maximum water level range of c. 5m at Lyttleton (de Lange & Healy 1986). Locally generated tsunami have several potential sources such as fault movement, submarine landslides, and volcanic eruptions associated with the Pacific–Australia plate boundary (de Lange & Fraser 1999). Historical local tsunami tend to be larger than remote tsunami and the maximum runup height identified from a palaeotsunami deposit is 32m above mean sea level (Nichol et al. 2003).

In a separate study, long wave resonances were evaluated along the coast of New Zealand using a frequency domain model (Walters 2002). Those results, coupled with historical and palaeotsunami data, provide a consistent picture of the temporal and spatial interaction between long waves and the coastal bathymetry (Walters & Goff 2003). That study in turn provided a general perspective from which we can now target smaller areas with local studies.

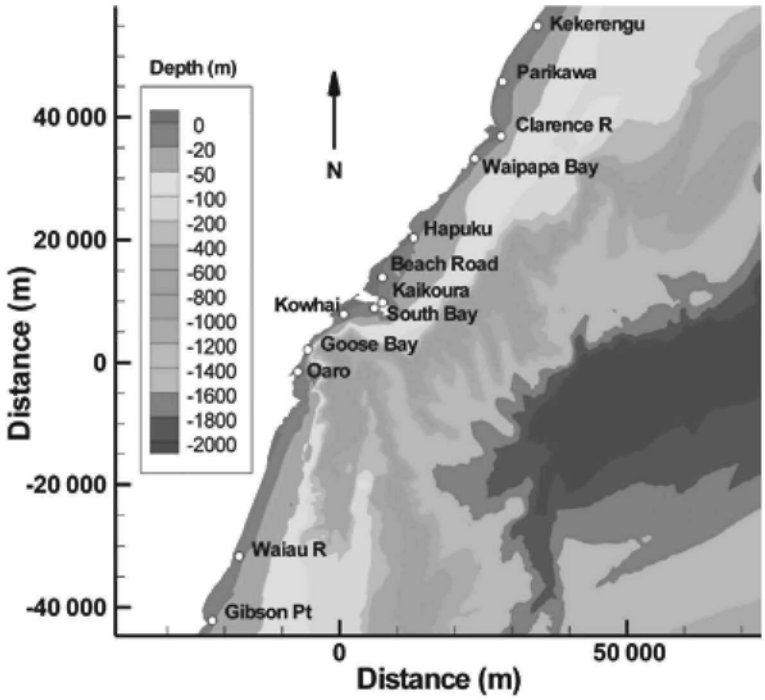

Fig. 1 Bathymetry of the study area including sites where time series of water level were recorded during the model simulations.

In this two-part paper, the focus was on determining the potential runup from local sources along the Kaikoura coastal margin (Fig. 1) as a result of fault ruptures (Part 1) and submarine landslides (Part 2).

There is a lack of substantive historical data for tsunami inundation along the Kaikoura coast north of the Kaikoura Peninsula. Work undertaken on prehistoric material, either archaeological or geological, gives no direct data of tsunami inundations but rather provides some circumstantial evidence for possible events. A Maori legend tells of a Taniwha (sea monster) that lived at the exit of Kaikoura Lagoon and used to rise up and kill Maori warriors on the spit from time to time (Elvy 1950). In the absence of any geological study there is no evidence to interpret such a legend.

A series of four uplifted beach ridges on the north side of Kaikoura Peninsula (Fig. 1) date to c. 200 years BP (1.1 m uplift), c. 400/500 years BP (0.8 m uplift), 1400 years BP (1.1 m uplift), and 1900 years BP (unknown uplift) (McFadgen 1987). There is a contemporaneous uplifted beach ridge for at least one of these events, and possibly more, in South Bay (Fig. 1) (Boorer 2002). This suggests that uplift of the whole Peninsula may have taken place at these times. The causative fault has not been identified, but is likely to be close by beneath the continental shelf or upper slope.

The general outline of this paper is as follows: the next section contains background information on the tectonic setting and the relevant tsunami generation mechanisms. Following that is a description of the model as currently developed as well as details about the coupling between the generation process and the fluid. Then we present a case study of local tsunami generated by fault ruptures near Kaikoura, on the east coast of the South Island, New Zealand.

GENERATION MECHANISMS

The Kaikoura coast lies in a tectonically complex, transitional setting within the centre of the Pacific–Australia plate boundary (Fig. 2). To the north, along the Hikurangi margin, the oceanic Pacific Plate is being subducted obliquely beneath North Island at c. 40–50 mm/yr (DeMets et al. 1994). Much of the shortening is accommodated on the plate interface and in the eastern margin (e.g., Lewis & Pettinga 1993; Barnes & Mercier de Lépinay 1997; Nicol & Beavan 2003), whereas motion parallel to the plate boundary is accommodated largely by strike-slip faulting in axial ranges of North Island (Kelsey et al. 1995; Van Dissen & Berryman 1996). To

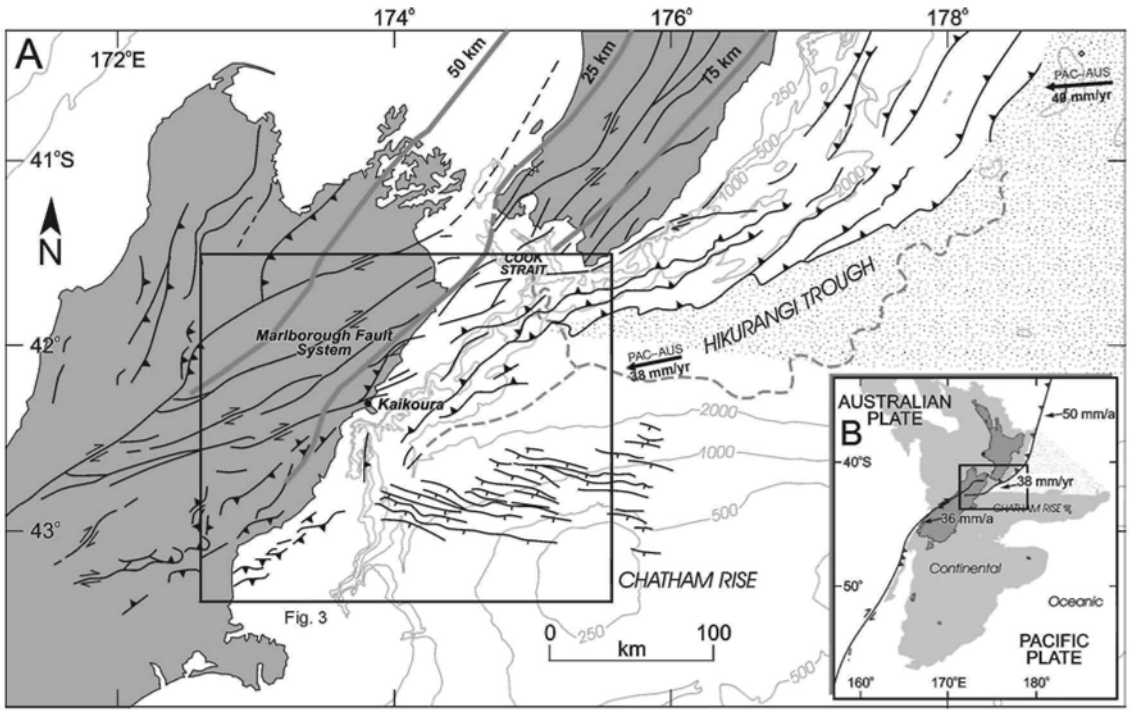

Fig. 2 **A**, Simplified tectonic map of central New Zealand (modified from Barnes et al. 1998), showing depths to the Benioff zone (bold contours, from Ansell & Bannister (1996) and Eberhart-Phillips & Reyners (1997)), and NUVEL-1A plate motions (DeMets et al. 1994). **B**, Map of the Pacific-Australia plate boundary in the New Zealand region.

the south, there is oblique continental collision in the central South Island, with plate motion accommodated by right-lateral and thrust displacement on the Alpine Fault, and thrust faulting along the eastern (Canterbury) margin of the Southern Alps (e.g., Norris et al. 1990).

The Kaikoura region is characterised by widespread historical seismicity associated with the subducted Pacific Plate and upper crustal rocks (Anderson & Webb 1994; Eberhart-Phillips & Reyners 1997; Reyners et al. 1997). Despite at least 200 km of total subduction revealed by the distribution of earthquakes beneath Marlborough, geological studies indicate that the plate motions are currently largely being accommodated by right-lateral strike-slip faulting that is distributed across the Marlborough Fault System (Lamb 1988; Cowan 1990; Van Dissen & Yeats 1991; Wood et al. 1994; Holt & Haines 1995; Little & Roberts 1997). These northeast-trending faults pass through the Kaikoura Ranges with slip rates in excess of 20 mm/yr, and some extend offshore beneath the continental margin north of Kaikoura Peninsula (Barnes & Audru 1999a,b). To the southeast, active reverse faults underlie the Marlborough continental slope (Barnes et al. 1998a). The north Canterbury region is dominated by thrust and reverse faults and folds (Fig. 2) (Nicol 1991; Pettinga et al. 2001). They flank the margins of large basins on land such as the Culverden and Cheviot Basins (Fig. 3), and are responsible for the uplift and local exposure of Mesozoic Torlesse basement rocks in coastal hills (Nicol 1991). Some active structures are hidden beneath the Canterbury Plains, whereas offshore the southeastern edge of the deformation zone underlies the north Canterbury continental shelf (Barnes 1996).

The Kaikoura coastline straddles an area with substantial vertical topographic and bathymetric relief, as well as considerable geological complexity (Fig. 3). The submarine trench marking the edge of the plate boundary, the Hikurangi Trough, shallows southwards along the toe of the Marlborough continental margin, and terminates in c. 2500 m water depth offshore of Kaikoura Peninsula. This occurs approximately where the c. 15-km-thick oceanic crust of the Hikurangi plateau intersects the thicker (c. 27 km) continental crust of the Chatham Rise (Fig. 2) (Reyners & Cowan 1993; Davy & Wood

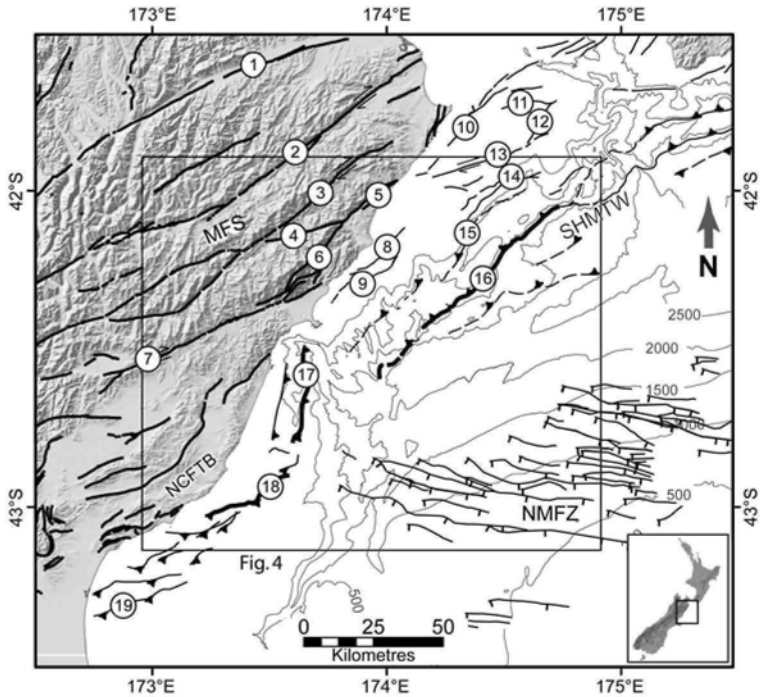

Fig. 3 Simplified map of active faults in the Marlborough region. (MFS, Marlborough Fault System; NCFTB, North Canterbury fold and thrust belt; NMFZ, North Mernoo Fault Zone; SHMTW, Southern Hikurangi margin thrust wedge.) Numbered faults include: (1) Wairau Fault; (2) Awatere Fault; (3) Clarence Fault; (4) Fidget Fault; (5) Kekerengu Fault; (6) Jordan Thrust; (7) Hope Fault; (8) Seaward segment; Hope Fault (9) Kaikoura Fault; (10) Needles Fault; (11) Boo Boo Fault; (12) Campbell Bank Fault; (13) Chancet Fault; (14) Te Rapa Fault; (15) Upper Slope Fault Zone; (16) Kekerengu Bank thrust; (17) Conway Ridge Fault; (18) North Canterbury shelf fault VIII (of Barnes 1996), (19) Pegasus Bay Fault. Offshore structures in bold were selected as potential tsunami sources for this study.

1994). At the southern end of the Hikurangi Trough, major submarine canyons incise the continental margin and are conduits for sediment transport from the Southern Alps to the Hikurangi Trough and beyond to the deep Pacific Basin (Lewis et al. 1998a). The Kaikoura Canyon is presently active because it intersects the modern sediment transport system in the nearshore region (Lewis & Barnes 1999). It is the potential instability of sediment at the head of this canyon that is examined in Part 2 of this paper.

Coseismic fault displacement as a potential tsunami source

The Kaikoura margin lies within a highly active region of the Pacific-Australian plate boundary, and future submarine earthquakes can be expected. Analysis of historical earthquake data indicates that despite the abundant seismicity in the subducted Pacific Plate beneath Marlborough, the subduction interface appears to be now locked permanently. The predicted plate boundary displacements can be largely accounted for on faults in Marlborough (Holt & Haines 1995), and no thrust earthquakes have been recorded at the plate interface (Reyners et al. 1997). Therefore, large magnitude, upper crustal strike-slip and thrust earthquakes, rather than subduction (interplate) earthquakes, might be expected in this region in the future (Pettinga et al. 2001; Stirling et al. 2001).

There are many active faults in the continental margin that either extend from onshore to offshore, or are entirely submarine. Based on fault dimensions and empirical scaling relationships (Wells & Coppersmith 1994), the largest faults off the Marlborough coast appear capable of generating large magnitude (>7) earthquakes. Slip rates on the most active strike-slip faults beneath the continental shelf likely exceed 10 mm/yr, from which we estimated recurrence intervals of thousands of years. Reverse faults beneath the Marlborough slope and north Canterbury shelf typically have slip rates of <0.2 mm/yr, and recurrence intervals may be several tens of thousands of years (Barnes 1996). To date, many of the submarine faults in the region have not been incorporated into current models of seismic hazard (Stirling et al. 2000; Pettinga et al. 2001), but work in this area is progressing.

It is the larger magnitude earthquakes capable of significant vertical coseismic deformation of the seabed that are of interest in assessing the potential for near-field tsunami generation by fault displacement. It is likely that earthquakes with magnitude of the order of >6.5 are required to rupture the seabed, and only the largest earthquakes in the area might be associated with surface displacements sufficient

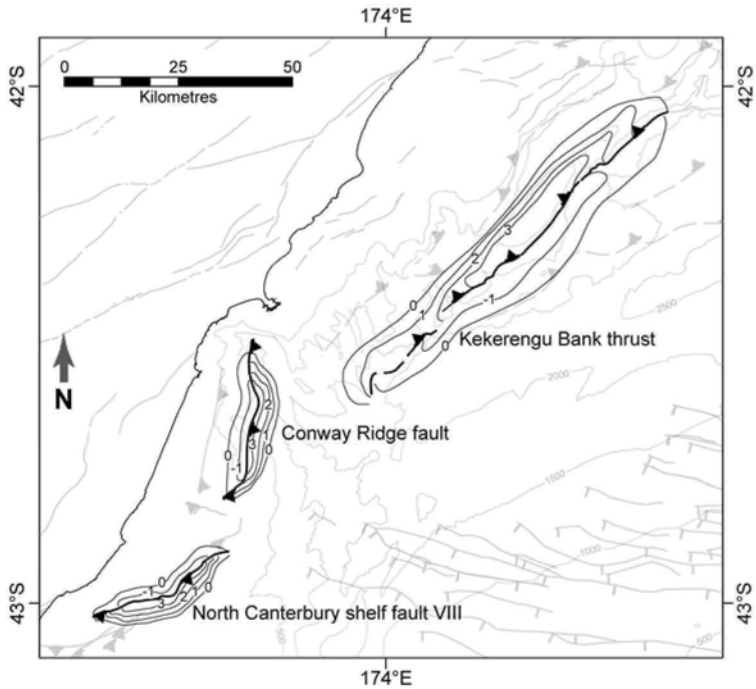

Fig. 4 Map of three potential fault displacement scenarios. Numbered contours are inferred uplift (positive) and subsidence (negative) values associated with an earthquake rupture on each fault. See text for derivation of displacement estimates.

to generate tsunami waves. The characterisation of potential tsunami sources requires an understanding of the earthquake potential and the expected coseismic displacement. Variations in the source parameters such as slip distribution, shear modulus at shallow depth, and rupture directivity might also be significant factors in the resulting propagation of tsunami waves (Okal 1988). For this preliminary study, we selected three potential reverse fault sources in the vicinity of the Kaikoura coast (Fig. 4), with potential for large vertical coseismic deformation of the seabed and with favourable orientations for directing tsunami waves at the coast. As the subduction interplate thrust beneath Marlborough is not considered to be currently active, it was not considered here as a potential tsunami source. The Hope and Kekerengu Faults were similarly not considered here, as they are principally steeply-dipping strike-slip faults with a subordinate component of vertical deformation (Barnes & Audru 1999a). The three fault sources considered include: (1) A 22 km long, northeast-dipping reverse fault beneath the Conway Ridge, lying in 200–700 m water depth. This fault has a slip rate that has not been constrained by stratigraphy, but appears from bathymetric expression to be of the order of 1 mm/yr or greater; (2) The northwest-dipping Kekerengu Bank thrust, lying in c. 1000–1500 m water depth beneath the Marlborough continental slope. This fault has accumulated up to 800–1000 m of vertical displacement of Pleistocene strata, and on the basis of its bathymetric expression, may have a slip rate of the order 0.5–1.5 mm/yr; (3) A southeast-dipping reverse fault beneath the north Canterbury shelf (fault VIII of Barnes (1996)), which has an estimated slip rate of <0.5 mm/yr, and lies in 40–120 m water depth.

Using the rupture area regression of Wells & Coppersmith (1994), and assuming a brittle crustal depth of 15 km and a conservative fault dip of 40–70°, the maximum credible earthquakes from these faults were estimated to be M_w 6.6–6.8 (Conway Ridge), M_w 7.1–7.3 (Kekerengu Bank), and M_w 6.8–6.9 (north Canterbury). Using a very simplistic approach for the purposes of this study, we estimated the potential coseismic displacements from two sources of information. First, seismic reflection profiles across the faults and bathymetric data were used to constrain the extent and pattern of late Quaternary uplift and subsidence, resulting from the long-term (i.e., many earthquake cycles) geological growth of folds associated with the faults. Secondly, empirical data relating coseismic displacements and fault rupture lengths were considered (Wells & Coppersmith 1994), together with historical data

on coseismic deformation patterns resulting from thrust earthquakes in New Zealand, such as the 1931 magnitude 7.8 Napier Earthquake (Hull 1990). In each source example, we assumed a maximum surface displacement of 3 m, which is in agreement with displacements assigned to similar structures in current New Zealand seismic hazard models (Stirling et al. 2000, 2001; Pettinga et al. 2001). The inferred surface patterns of coseismic deformation were then sketched around the structures, with a zero deformation contour positioned to coincide with the zero long-term geological deformation contour (Fig. 4). These simple models can be tested in future work using simple elastic dislocation modelling of the potential displacements, or more complex modelling of the tsunami sources.

MODEL DESCRIPTION

The numerical model used is a general-purpose hydrodynamics and transport model known as RiCOM (River and Coastal Ocean Model). The model has been under development for several years and has been evaluated and verified continually during this process (Walters & Casulli 1998; Walters 2004, 2005). The hydrodynamics part of this model was used to derive the results described in the next section.

The model is formulated from the Reynolds-averaged Navier-Stokes equations (RANS) with a free surface so that the dependent variables are time-averaged over turbulent time scales. For the simulation of weakly dispersive surface waves, these equations are averaged over water depth to derive a set of equations similar to the standard shallow water equations but containing additional terms that describe non-hydrostatic forces (Stelling & Zijlema 2003; Walters 2005).

The free surface equation is derived by vertically integrating the continuity equation:

$$\frac{\partial \eta}{\partial t} + \nabla \cdot (H\mathbf{u}) = 0 \tag{1}$$

where ∂ denotes a partial derivative, $\eta(x,y,t)$ is the water-surface elevation measured from the vertical datum, t is time, ∇ is the horizontal gradient operator, $\cdot$ is the vector dot product, $\mathbf{u}$ is the depth-averaged velocity, $h(x,y)$ is the land elevation measured from the vertical datum, and $H = \eta(x,y,t) - h(x,y)$ is the water depth. The vertical datum is arbitrary, but is usually set equal to the average water surface elevation (sea level). This choice minimises truncation errors in the calculation of the water surface gradients.

After depth-averaging, the horizontal momentum equation becomes:

$$\frac{D\mathbf{u}}{Dt} + \mathbf{f} \times \mathbf{u} = -g\nabla\eta - \frac{1}{2}\nabla(q) - \frac{q}{2H}(\nabla\eta + \nabla h) + \frac{1}{H}\nabla \cdot (HA_h\nabla\mathbf{u}) - \frac{\tau_b}{\rho H} \tag{2}$$

where D/Dt is a material derivative, $\mathbf{f}$ is a vector representation of the Coriolis parameter, q is dynamic pressure which varies linearly in the vertical with $q = 0$ at the free surface, A_h is horizontal eddy viscosity, τ_b is bottom friction, and ρ is density. Surface stress and atmospheric pressure were neglected. Bottom friction is written as:

$$\frac{\tau_b}{\rho H} = -\frac{C_D|\mathbf{u}|\mathbf{u}}{H} = \gamma\mathbf{u} \tag{3}$$

where C_D is a drag coefficient and γ is defined by Equation 3. Equations 1 and 2 with $q = 0$ form the classical shallow water equations.

Next, the vertical momentum equation and the continuity equation must be depth averaged to derive governing equations for vertical velocity w and dynamic pressure q. The former is:

$$\frac{Dw}{Dt} = -\frac{(q_\eta - q_h)}{H} = \frac{q_h}{H} \tag{4}$$

where w is the depth-averaged vertical velocity, q_η is dynamic pressure at the free surface, q_h is dynamic pressure at the bottom, and the vertical viscous terms have been neglected. The vertically integrated continuity equation is expressed as:

$$\int_h^\eta \nabla \cdot \mathbf{u} dz + w_\eta - w_h = 0 \tag{5}$$

This equation is written in finite volume form when it is discretised.

To allow flexibility in the discretisation of the model grid across the continental shelf, finite elements with unstructured triangular and quadrilateral elements of varying-size and shape were used for the spatial approximation. The time marching algorithm is a semi-implicit scheme that removes stability constraints on wave propagation (Casulli & Cattani 1994). The advection scheme is semi-Lagrangian which is robust, stable, and efficient (Staniforth & Côté 1991). Wetting and drying of intertidal or flooded areas occurs naturally with this formulation and is a consequence of the finite volume form of the continuity equation and method of calculating fluxes through the element faces. At open (sea) boundaries, a radiation condition was enforced so that the outgoing wave did not reflect back into the modelled area.

The equations are solved with a split-step method. In the first step, the equations are solved with $q = 0$ to derive an approximate solution for the dependent variables (Walters & Casulli 1998). In the second step, an equivalent of a pressure Poisson equation is solved for q and the velocity solution from step one is corrected (Walters 2005).

This method can be expanded in a straightforward manner to three dimensions when greater accuracy is required (Stelling & Zijlema 2003) and provides an alternative to the Boussinesq equations which use higher order velocity and geometry correction terms in the momentum equation (Lynett & Liu 2002).

Model grid and bathymetry

The bathymetric data were compiled from several sources and are summarised in Lewis et al. (1998b). The depths in deeper water were measured during a swath survey from the French (IFREMER) R.V. *L'Atalante* using a Simrad EM1 12D swath mapping system in November 1993. Nearshore launch surveys were made using echosounders and side-scan sonar with positioning by differential global positioning system (GPS) in April and December 1996. Other soundings were from R.V. *Rapuhia* surveys in 1988–92, from digitised charts (LINZ 2005), and other bathymetric sources (Barnes et al. 1998b).

The combined land and seabed topographic database was used to derive a reference elevation grid. Some parts of the grid were defined on a regular mesh such as the bathymetric data with 25 and 50 m grid spacing. Other parts such as the land topography were defined on an irregular grid that was derived from LINZ shoreline data (LINZ 2005), the 20 m elevation contour, and GPS survey points by using a direct triangulation of the data points. The topography for nodes in the model grid was interpolated from these reference grids.

The model grid has a number of requirements that ensure that the model calculations are accurate and free of excessive truncation errors (Henry & Walters 1993). The primary requirements are that the triangular elements are roughly equilateral in shape and their grading in size is smooth from areas of high resolution (small elements) to areas of low resolution (large elements).

The model grid was generated in two parts that were separated by the LINZ shoreline contour. The land and ocean grids were joined at the points along the shoreline resulting in the complete model grid. This grid was subsequently refined, resulting in a grid spacing of c. 80 m along the shoreline. The element size increased gradually out to c. 400 m along the ocean boundary. The smaller element size in shallow water was necessary to resolve the slower wave speed and shorter wavelength for shoaling tsunami waves. We verified in the results that the refinement was adequate to resolve the tsunami that are generated. Elevations in the final model grid were interpolated from the reference grids. The final grid contains 513 284 nodes and 1 021 434 elements.

Initial conditions

For the type of fault ruptures considered in this study, fault movement is assumed to be rapid when compared to time scales for wave propagation. Thus, owing to the incompressible nature of water, the instantaneous initial conditions on the water surface were the same as the fault displacement. This modelling strategy was adopted for the three fault rupture scenarios identified earlier. Essentially, the tsunami started with zero velocity and a surface displacement given by the estimates for seabed rupture, and the wave evolved in time as a long gravity wave. At the open (sea) boundaries, a radiation condition was enforced so that the outgoing wave did not reflect back into the modelled area.

Following the nomenclature in the section on the tectonic setting, the northern fault is denoted as the Kekerengu Bank fault (KBF), the central fault as the Conway Ridge fault (CRF), and the southern fault as the North Canterbury fault (NCF). The displacements for these faults in terms of initial water surface elevation are shown in Fig. 4. The former, KBF, has the largest spatial extent and directs a tsunami straight towards the Clarence River area. Because the displacement is upward on the landward side, the initial wave along the coast was a peak rather than an initial drawdown. The other two faults, CRF and NCF, have displacements in the opposite sense so the initial wave was an N-wave or wave trough.

RESULTS AND DISCUSSION

The study area spanned the distance from Oaro in the south to Kekerengu in the north (Fig. 1). The more important developed sites are Oaro, Goose Bay, South Bay, and Kaikoura. The area is characterised as an uplifted beach platform with local areas of sediment accumulation such as Clarence River and Oaro (Ota et al. 1996). Hence, the area has relatively high exposure to incident tsunami.

In the context used here, the amplitude of tsunami waves is the level of the wave crest and trough for simple waves reached respectively above and below

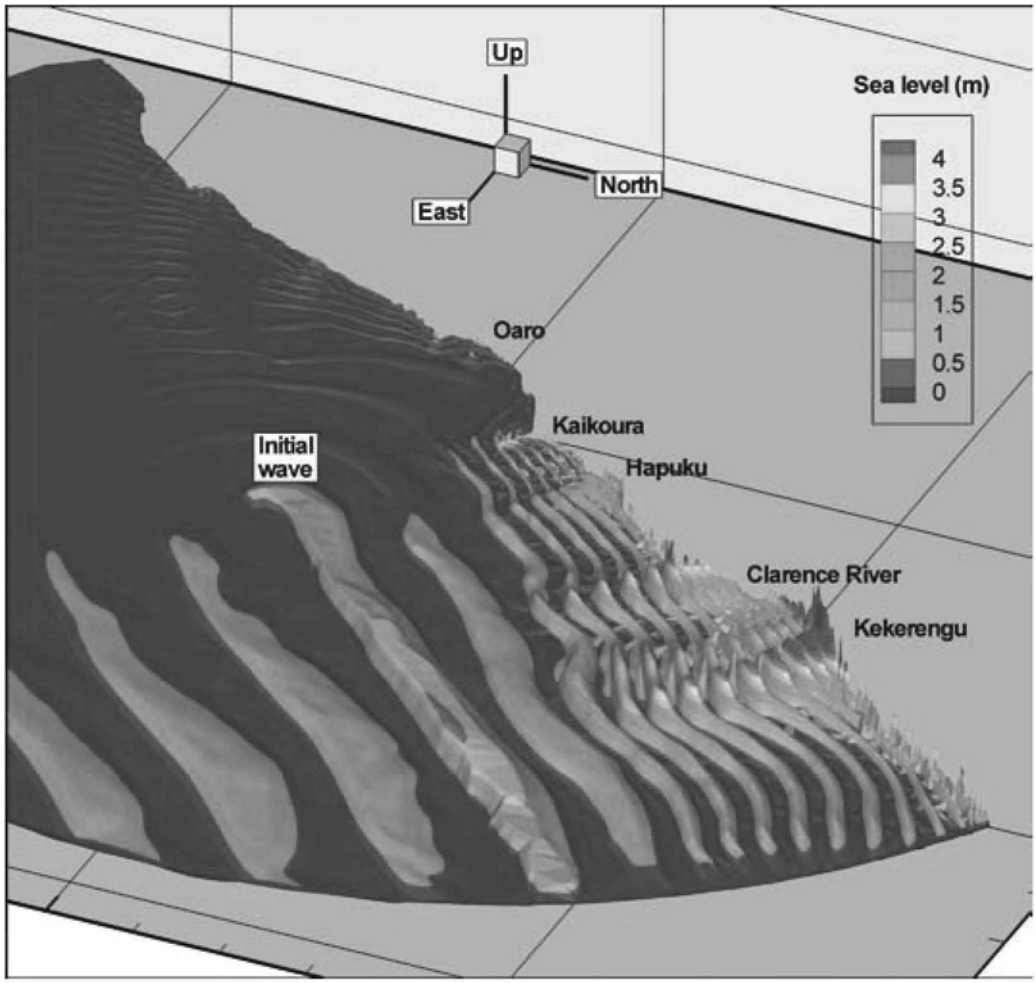

Fig. 5 Time sequence of water levels at 100-s intervals for a tsunami generated by a Kekerengu Bank fault-rupture. The entire semicircular model domain is shown with Kaikoura Peninsula at the circle's centre.

the tide level at the time. The wave height from crest to trough is therefore twice the amplitude or range. However, in shallower water, the wave distorts, so what is reported here is the vertical height reached by the wave crest, being the most relevant to the inundation hazard. At the landward extent of inundation, the wave height is equivalent to the runup height.

The initial waveform for fault movement events was modelled as a wave with surface elevation that is the same as the fault displacement and had zero velocity. Based on simple physics, this wave decomposes into a combination of two waves travelling in opposite directions so that the wave velocity sums to zero. Thus the initial wave split into two waves—one travelling offshore and one travelling onshore, each with about half the original amplitude (Fig. 5). For a wave with a long and straight wave crest such as those generated by long fault ruptures, the amplitude would be maintained, subject to variations in water depth. Only the ends of the wave would tend to decrease in amplitude as they radiate in circular patterns (Fig. 5). Waves that are generated as point sources, such as the landslide event, tend to lose amplitude as they also radiate away in circular patterns (see Part 2, Walters et al. this issue, fig. 3).

When waves encounter shallow water, the speed of the crests and troughs (phase speed) decreases. Thus the wavelength becomes shorter and the amplitude increases. If the wave encounters a sloping beach, the runup height can be up to approximately four times the initial wave amplitude (Synolakis 1987) and the wave undergoes partial reflection. If the wave

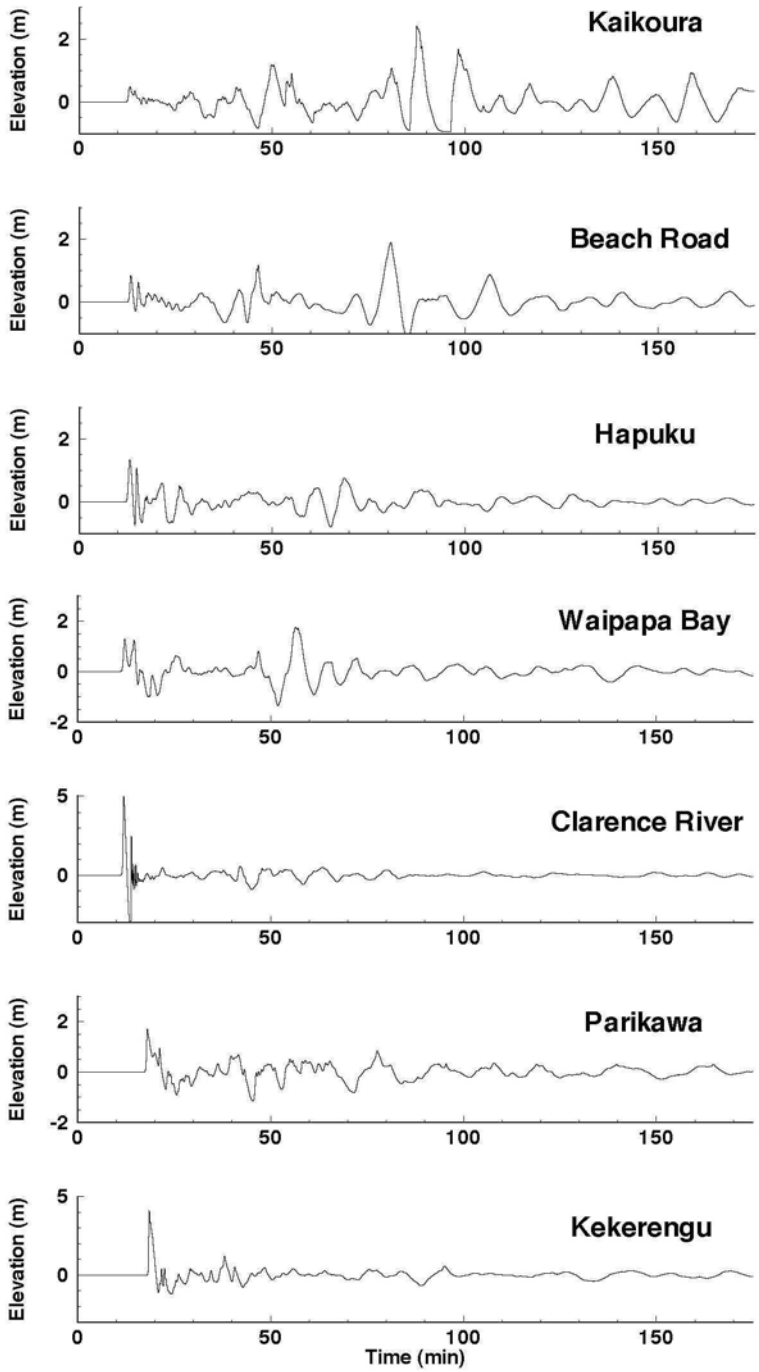

Fig. 6 Time series of water levels after the Kekerengu Bank fault-rupture event for the sites defined in Fig. 1.

encounters a vertical cliff, the wave is completely reflected and the amplitude at the cliff is twice the incident wave amplitude (superimposed incident and reflected wave). This creates a standing wave where the reflection occurs, and is a common occurrence in many of the coastal inlets and bays (e.g., Fig. 5). Most of these phenomena are readily apparent in the results for the northernmost fault scenario when the wave propagates straight in to the coast north of Clarence River (Fig. 5).

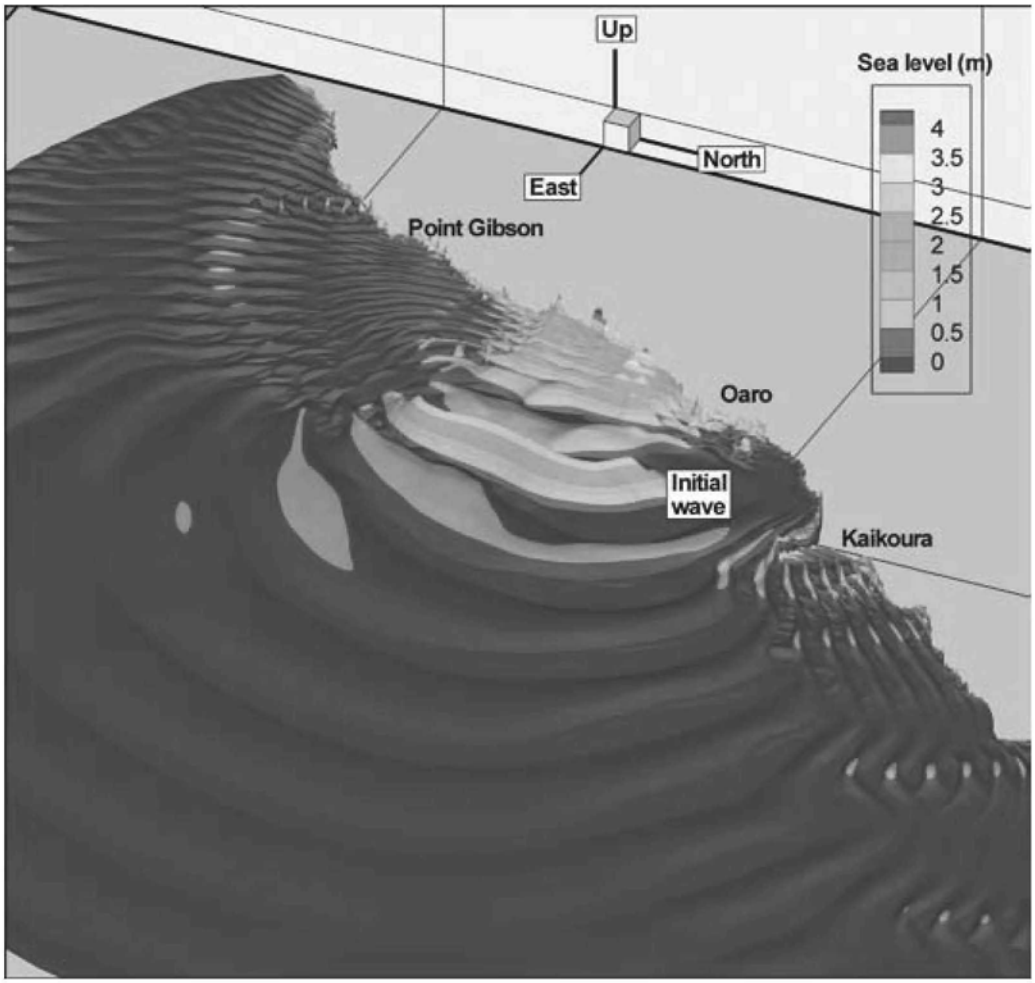

Fig. 7 Time sequence of water levels at 250-s intervals for a tsunami generated by a Conway Ridge fault-rupture.

In addition, wave refraction occurs if the wave front straddles areas with different water depths at each end of the wave front. Because the wave travels more slowly in shallow water, the wave front tends to bend around toward the gradient in depth. For a long straight beach, obliquely incident waves then tend to become parallel to the shore. By the same process, waves travelling along the shoreline will tend to be trapped because the offshore component of the wave travels faster and hence refracts back toward the shore. These coastal-trapped waves were common in the results and are important in understanding why moderate to large waves can occur at some distance along the coast from the local rupture site long after the direct wave has passed (Fig. 5 and 6 at Kaikoura).

When a wave is generated, all these processes occur simultaneously along the coast, leading to complicated wave patterns. The trapped waves are reflected by the irregular coastline and then traverse the entire coast, back and forth. When these waves resonate in small bays, there can be large amplitude waves that occur long after the waves were initially generated. For instance, these waves are a common occurrence at Kaikoura township (Fig. 6).

Fault movement events —Kekerengu Bank Fault

The northern fault, KBF, has the largest spatial extent and directs a tsunami straight towards the Kekerengu area (Fig. 5). The initial wave separated into two waves of approximately half the initial amplitude—one directed toward the coast, the other directed offshore to become a remote tsunami elsewhere. For the landward-directed wave, the wavelength

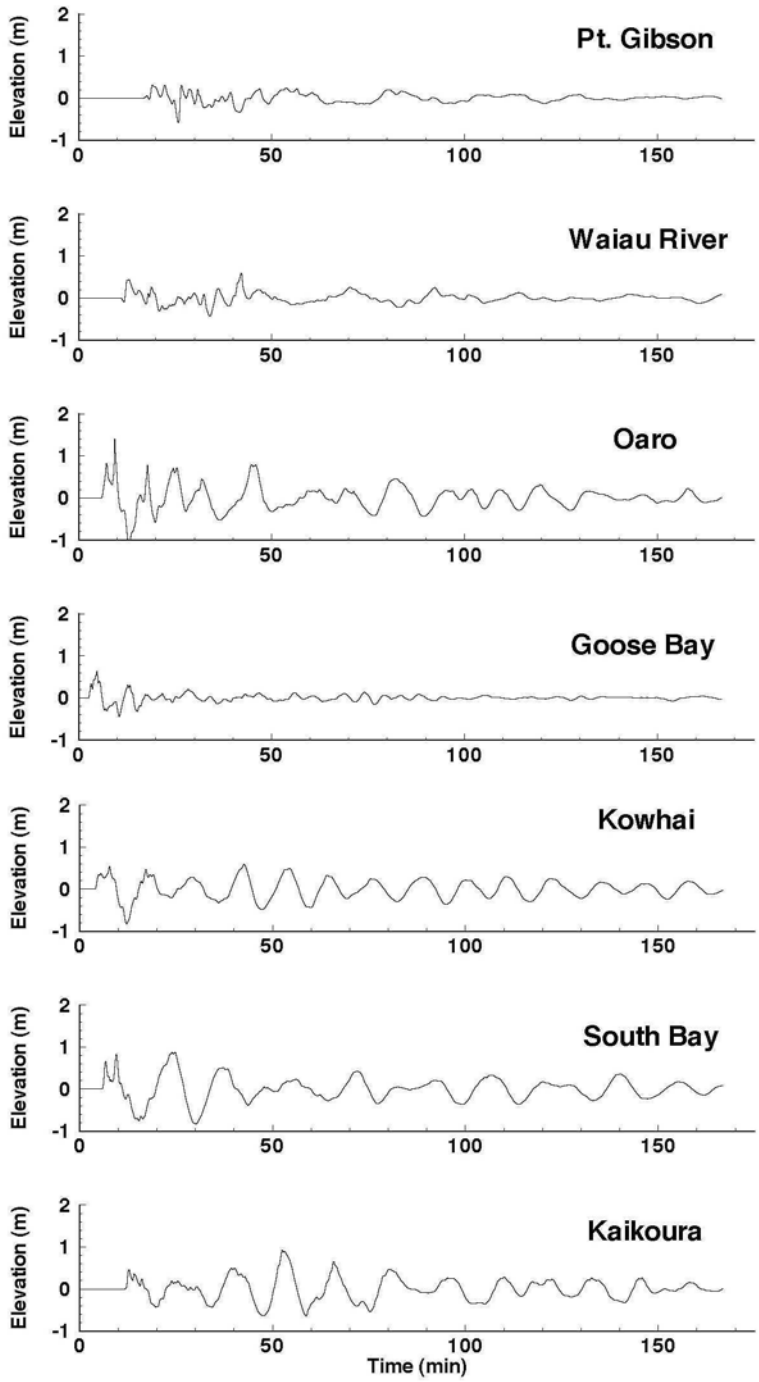

Fig. 8 Time series of water levels after the Conway Ridge fault-rupture event for the sites defined in Fig. 1.

decreased and the wave height increased as the water depth decreased (Fig. 5). After c. 10 min, the tsunami reached the Clarence River where the wave crest height reached c. 5 m above the tide level. The Clarence River delta was inundated for several minutes and water speed on land was c. 10 m/s. Shortly thereafter, the main part of the wave ran up to the north at Parikawa and Kekerengu. There was considerable inundation of the coastal platform south of Kekerengu. There were also a

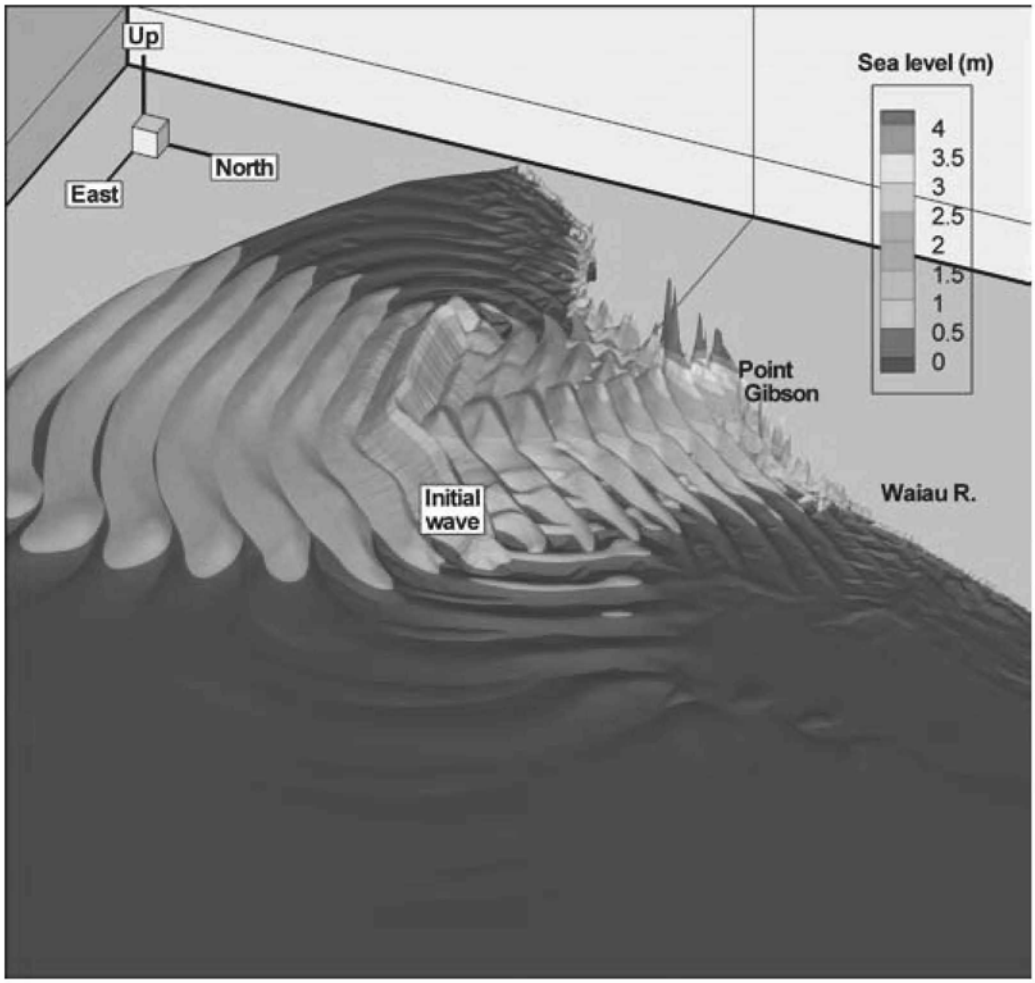

Fig. 9 Time sequence of water levels at 250-s intervals for a tsunami generated by a North Canterbury fault-rupture.

number of reflections and the secondary waves were partially refracted to form coastal-trapped waves that propagated both north and south. The characteristic wave period for the coastal-trapped waves was c. 12 min as compared with a period of c. 1 min for the incident wave. The southward travelling waves underwent numerous reflections to create a series of waves travelling both north and south that persisted for over 3 h with reducing wave heights. There appeared to be a resonance around Kaikoura with a relatively high wave crest (2.5 m) occurring 1.5 h after the fault-rupture event (Fig. 6). The response south of Kaikoura Peninsula was much smaller with the highest wave crests being 0.2 to 0.8 m above the tide level (Fig. 6).

Fault movement events—Conway Ridge Fault

The central fault, CRF, lies on the Conway Ridge offshore from Oaro. This fault is smaller in spatial extent than the northern fault and has a reverse pattern with uplift away from shore, thereby creating a trough on the landward side of the wave (Fig. 7). However, the negative wave front propagated south of Oaro so that for all the sites in the study area the initial wave had a positive peak. The main part of the tsunami reached shore between the Waiau River and Oaro c. 7 min after the fault rupture and the wave crest height was 2 m above the tide level. Maximum wave crest heights of 0.7 m occurred at Oaro, Goose Bay, and South Bay. North of Kaikoura Peninsula wave crest heights were generally small

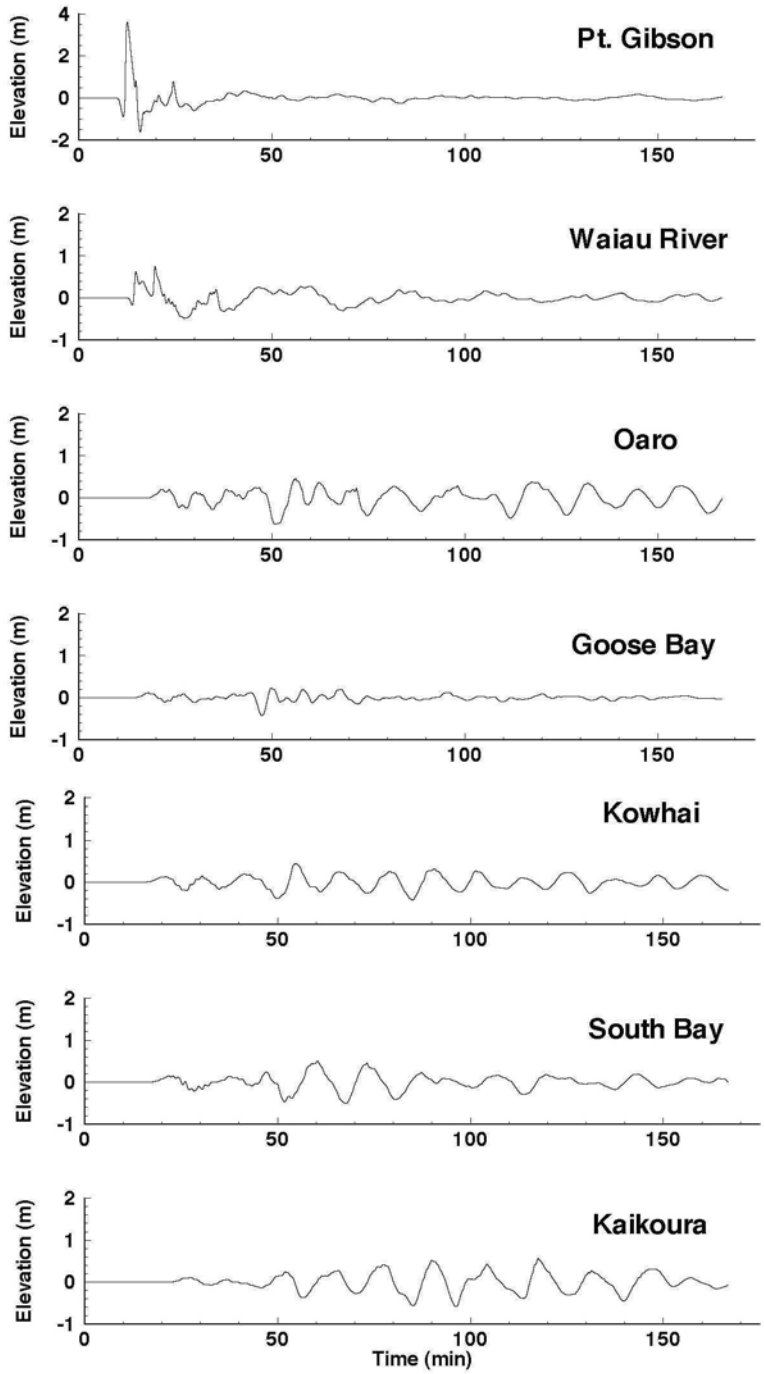

Fig. 10 Time series of water levels after the North Canterbury fault-rupture event for the sites defined in Fig. 1.

(0.2 m or less) except at Kaikoura where a resonance was again excited (Fig. 8). There the wave crest reached slightly over 1 m c. 50 min after the rupture event (Fig. 8).

Fault movement events —North Canterbury Fault

The southern fault, NCF, primarily affected the area south of the main study area (Fig. 9). The

main part of the tsunami reached shore near Point Gibson c. 10 min after the fault rupture and the maximum wave height was 3.6 m at 12.5 min after the rupture. In the study area, the initial wave had a crest height of up to 0.25 m south of Kaikoura Peninsula and smaller elsewhere (Fig. 10). However, there were much larger secondary waves caused by reflections and coastal-trapped waves with crest heights reaching 0.45 m at South Bay. Again, a resonance occurred at Kaikoura with oscillations up to 0.5 m high that started c. 1 h after the rupture event and lasted for several hours. Elsewhere north of Kaikoura Peninsula, the crest heights were small (less than 0.15 m) (Fig. 10).

CONCLUSION

For the fault-rupture events considered here, the northern coast of the study area was very exposed to damage from a potential rupture of the Kekerengu Bank Fault. The wave crest heights for the Kaikoura area were moderate (although the consequences may be higher owing to the greater value of the built environment), decreasing to small crest heights south of Kaikoura Peninsula for fault-rupture mechanisms. A potential concern is that the highest waves near Kaikoura would be a result of late arrival of coastally-trapped waves and would be delayed by up to 1.5 h from the fault-rupture event.

It is regrettable that there has been no comprehensive geological survey of the area for palaeotsunami deposits. In the absence of these data we are limited to a Maori legend reported by Elvy (1950) and to uplift of the Peninsula that may or may not have been tsunamigenic. Given the likely significance of these events for Kaikoura township, it would seem appropriate to investigate the palaeotsunami record of the old Kaikoura Lagoon which has been filled in and is under mixed farmland and housing.

The fault-rupture scenarios chosen here were selected because of their potentially large impacts, yet retaining events that could be realistically possible. The pattern of exposure reflects the fact that there is a large fault directly offshore of the northern part of the study area, and that this fault is oriented such that it propagates an initial wave crest directly into the coast. The faults identified in the southern part of the study area propagated waves at an oblique angle or out of this area and hence had a lesser effect.

We have chosen examples that maximise the length and height of the tsunami by assuming that the fault displacement will be over the entire length of the fault and at the maximum reasonable amplitude. Although the values chosen are reasonable, there is considerable uncertainty over the size and surface distribution of displacement that would actually occur in a given event. The amplitude may be up to c. 30% higher, or it could be much lower. The wave crest height of a tsunami scales with the fault amplitude so this provides a rough guide to gauge effects at the coast. In the example of the Kekerengu Bank Fault, the length of the fault rupture may also be smaller than was considered here. This would lead to a more local effect of the initial waves, and perhaps a reduction in surface displacement.

In addition, most of the tsunami scenarios were characterised by short response times. For the fault-generated tsunami, waves generally started reaching the coast within 10 min after the event.

Finally, there could be multiple-related hazard events (probably the most common example). For instance, a local earthquake can cause a locally-generated tsunami, and there may be multiple tsunami generated by both a fault rupture and underwater landslide. There may also be confounding effects from high wave/storm activity and high tides.

ACKNOWLEDGMENTS

This research was partially funded by the New Zealand Foundation for Research, Science and Technology under contract CO1X0024. The application of this research to the assessment of tsunami hazards along the Kaikoura coast was partially funded by Environment Canterbury (Ecan).

REFERENCES

Anderson H, Webb T 1994. New Zealand seismicity: patterns revealed by the upgraded National Seismograph Network. New Zealand Journal of Geology and Geophysics 37: 477–493.

Ansell JH, Bannister SC 1996. Shallow morphology of the subducted plate along the Hikurangi margin, New Zealand. Physics of the Earth and Planetary Interiors 93: 3–20.

Barnes PM 1996. Active folding of Pleistocene unconformities on the edge of the Australian–Pacific plate boundary zone, offshore North Canterbury, New Zealand. Tectonics 15: 623–640.

Barnes PM, Audru J-C 1999a. Recognition of active strike-slip faulting from high-resolution marine seismic reflection profiles: Eastern Marlborough fault system, New Zealand. Geological Society of America Bulletin 111: 538–559.

Barnes PM, Audru J-C 1999b. Quaternary faulting in the offshore Flaxbourne and Wairarapa Basins, southern Cook Strait, New Zealand. New Zealand Journal of Geology and Geophysics 42: 349–367.

Barnes PM, Mercier de Lépinay B 1997. Rates and mechanics of rapid frontal accretion along the very obliquely convergent southern Hikurangi margin, New Zealand. Journal of Geophysical Research 102: 24931–24952.

Barnes PM, Mercier de Lépinay B, Collot J-Y, Delteil J, Audru J-C 1998a. Strain partitioning in a transition zone from oblique subduction to oblique continental collision: structural variations along the offshore southern Hikurangi margin, New Zealand. Tectonics 17: 534–557.

Barnes PM; Mercier de Lépinay B; Collot J-Y; Delteil J; Audru J-C, and GeodyNZ team 1998b. South Hikurangi GeodyNZ swath maps: depths, texture and geological interpretation. 1:500,000. New Zealand Oceanographic Institute Chart, Miscellaneous Series 75. Wellington, National Institute of Water and Atmospheric Research Limited.

Boorer S 2002. Geomorphic evolution of the South Bay coast, Kaikoura. Unpublished MSc thesis, University of Canterbury, Christchurch, New Zealand.

Casulli V, Cattani E 1994. Stability, accuracy, and efficiency of a semi-implicit method for three-dimensional shallow water flow. Computers Mathematical Applications 27(4): 99–112.

Cowan HA 1990. Late Quaternary displacements on the Hope Fault at Glynn Wye, North Canterbury. New Zealand Journal of Geology and Geophysics 33: 285–293.

Davy BW, Wood R 1994. Gravity and magnetic modelling of the Hikurangi Plateau. Marine Geology 128: 139–151.

de Lange WP, Fraser RJ 1999. Overview of tsunami hazard in New Zealand. Tephra 17: 3–9.

de Lange WP, Healy T 1986. New Zealand tsunamis 1840–1982. New Zealand Journal of Geology and Geophysics 29: 115–134.

DeMets C, Gordon RG, Argus DF, Stein S 1994. Effect of recent revisions to the geomagnetic reversal time scale on estimates of current plate motions. Geophysical Research Letters 21: 2191–2194.

Eberhart-Phillips D, Reyners M 1997. Continental subduction and three-dimensional crustal structure: The northern South Island, New Zealand. Journal of Geophysical Research 102: 11843–11861.

Elvy WJ 1950. Kaikoura coast: the history, traditions and Maori place-names of Kaikoura. Christchurch, Hundalee Scenic Board and Whitcombe and Tombs Ltd. 135 p.

Henry RF, Walters RA 1993. A geometrically-based automatic generator for irregular triangular networks. Communications in Applied Numerical Methods 9: 555–566.

Holt WE, Haines AJ 1995. The kinematics of northern South Island, New Zealand, determined from geological strain rates. Journal of Geophysical Research 100: 17991–18010.

Hull AG 1990. Tectonics of the 1931 Hawke Bay earthquake. New Zealand Journal of Geology and Geophysics 33: 309–320.

Kelsey HM, Cashman SM, Beanland SM, Berryman KR 1995. Structural evolution along the inner forearc of the obliquely convergent Hikurangi margin, New Zealand. Tectonics 14: 1–18.

Lamb S 1988. Tectonic rotations about vertical axes during the last 4 Ma in part of the New Zealand plate-boundary zone. Journal of Structural Geology 10: 875–893.

Lewis KB, Barnes PM 1999. Kaikoura Canyon, New Zealand: active sediment conduit from near-shore sediment zones to trench-axis channel. Marine Geology 162: 39–69.

Lewis KB, Pettinga JR 1993. The emerging, imbricated frontal wedge of the Hikurangi margin. In: Balance PF ed. South Pacific Sedimentary Basins: sedimentary basins of the world, 2. New York, Elsevier Science. Pp. 225–250.

Lewis KB, Collot J-Y, Lallemand SE 1998a. The dammed Hikurangi Trough: a channel-fed trench blocked by subducting seamounts and their wake avalanches (New Zealand–France GeodyNZ). Basin Research 10: 441–468.

Lewis KB, Garlick RD, Dawson SM 1998b. Kaikoura Canyon: depths, shelf texture, and whale dives. NIWA Chart Miscellaneous Series 78. Wellington, National Institute of Water and Atmospheric Research Limited.

LINZ 2005. New Zealand Chart Catalogue, Land Information New Zealand. http://www.hydro.linz.govt.nz/charts/catalogue/index.asp [accessed 15 June 2005].

Little TA, Roberts AP 1997. Distribution and mechanism of Neogene to present-day vertical axis rotations, Pacific-Australian plate boundary, South Island, New Zealand. Journal of Geophysical Research 102: 20,447–20,468.

Lynett P, Liu P 2002. A numerical study of submarine-landslide-generated waves and run-up. Proceedings of the Royal Society of London A 458: 2885–2910.

McFadgen B 1987. Beach ridges, breakers and bones: late Holocene geology and archaeology of the Fyffe site, S49/46, Kaikoura Peninsula, New Zealand. Journal of the Royal Society of New Zealand 17: 381–394.

Nichol S, Goff J, Regnauld H 2003. Cobbles to diatoms: facies variability in a paleo-tsunami deposit. Proceedings of the Coastal Sediments 2003 "Crossing Disciplinary Boundaries". The Fifth International Symposium on Coastal Engineering and Science of Coastal Sediment Processes, Florida, United States. Pp. 1–11.

Nicol A 1991. Structural styles and kinematics of deformation on the edge of the New Zealand plate boundary zone, mid Waipara region, north Canterbury. Unpublished PhD thesis, University of Canterbury, Christchurch, New Zealand.

Nicol A, Beavan J 2003. Shortening of an overriding plate and its implications for slip on a subduction thrust, central Hikurangi margin, New Zealand. Tectonics 22(6): 1070 [doi:10.1029/2003TC001521 (9– 1–14)].

Norris RJ, Koons PO, Cooper AF 1990. The obliquely-convergent plate boundary in the South Island of New Zealand: implications for ancient collision zones. Journal of Structural Geology 12: 715–725.

Okal EA 1988. Seismic parameters controlling far-field tsunami amplitudes: a review. Natural Hazards 1: 67–96.

Ota Y, Pillans B, Berryman K, Beu A, Fujimori T, Miyauchi T, Berger G 1996. Pleistocene coastal terraces of Kaikoura Peninsula and the Marlborough coast, South Island, New Zealand. New Zealand Journal of Geology and Geophysics 39: 51–73.

Pettinga JR, Yetton MD, Van Dissen RJ, Downes G 2001. Earthquake source identification and characterisation for the Canterbury region, South Island, New Zealand. Bulletin of the New Zealand Society for Earthquake Engineering 34: 282–317.

Reyners M, Cowan HA 1993. The transition from subduction to continental collision: crustal structure in the north Canterbury region, New Zealand. Geophysical Journal International 125: 1224–1236.

Reyners M, Robinson R, McGinty P 1997. Plate coupling in the northern South Island and southernmost North Island, New Zealand, as illuminated by earthquake focal mechanisms. Journal of Geophysical Research 102: 15,197–15,210

Staniforth A, Côté J 1991. Semi-Lagrangian integration schemes for atmospheric models—a review. Monthly Weather Review 119: 2206–2223.

Stelling G, Zijlema M 2003. An accurate and efficient finite-difference algorithm for non-hydrostatic free-surface flow with application to wave propagation. International Journal for Numerical Methods in Fluids 43: 1–23.

Stirling M, McVerry G, Berryman K, McGinty P, Villamor P, Van Dissen R, Dowrick D, Cousins J, Sutherland R 2000. Probabilistic seismic hazard assessment of New Zealand. New active fault data, seismicity data, attenuation relationships and methods. Institute of Geological and Nuclear Sciences. 113 p.

Stirling M, Pettinga JR, Berryman K, Yetton MD 2001. Probabilistic seismic hazard assessment of the Canterbury region, New Zealand. Bulletin of the New Zealand Society for Earthquake Engineering 34: 318–334.

Synolakis 1987. The runup of solitary waves. Journal of Fluid Mechanics 185: 523–545.

Van Dissen RJ, Berryman KR 1996. Surface rupture earthquakes over the last ~1000 years in the Wellington region, New Zealand, and implications for ground shaking hazard. Journal of Geophysical Research 101: 5999–6019.

Van Dissen R, Yeats RS 1991. Hope fault, Jordan thrust, and uplift of the seaward Kaikoura Range, New Zealand. Geology 19: 393–396.

Walters RA 2002. Long wave resonance on the New Zealand coast. NIWA Technical Report 109. National Institute of Water and Atmospheric Research Ltd. 32 p.

Walters RA 2004. Tsunami generation, propagation, and runup. Estuarine and Coastal Modeling. In: Spaulding ML ed. Proceedings of the 8th International Conference, American Society of Civil Engineers. Pp. 423–438.

Walters RA 2005. A semi-implicit finite element model for non-hydrostatic (dispersive) waves. International Journal for Numerical Methods in Fluids 49: 721–737.

Walters RA, Casulli V 1998. A robust, finite element model for hydrostatic surface water flows. Communications in Numerical Methods in Engineering 14: 931–940.

Walters R, Goff J 2003. Assessing tsunami hazard along the New Zealand coast. Science of Tsunami Hazards 21(3): 137–153.

Wells DL, Coppersmith KJ 1994. New empirical relationships among magnitude, rupture length, rupture width, rupture area, and surface displacement, Bulletin of the Seismological Society of America 84: 974–1002.

Wood RA, Pettinga JR, Bannister S, Lamarche G, McMorran TJ 1994. Structure of the Hamner strike-slip basin, Hope fault, New Zealand. Geological Society of America Bulletin 106: 1459–1473.